JOURNAL OF GEOPHYSICAL RESEARCH, VOL. 106, NO. C5, PAGES 9057–9073, MAY 15, 2001

Sea ice transports in the Weddell Sea

Sabine Harms,[1] Eberhard Fahrbach, and Volker H. Strass

Alfred-Wegener-Institut für Polar- und Meeresforschung, Bremerhaven, Germany

Abstract. Time series of sea ice draft in the Weddell Sea are evaluated together with hydrographic observations, satellite passive microwave data, and ice drift for estimation of the freshwater fluxes into and out of the Weddell Sea. Ice draft is measured with moored upward looking sonars since 1990 along two transects across the Weddell Gyre. One transect, extending from the tip of the Antarctic Peninsula to Kapp Norvegia, was sampled between 1990 and 1994 and covers the flow into and out of the southern Weddell Sea. The other transect, sampled since 1996 and extending from the Antarctic continent northward along the Greenwich meridian, covers the exchange of water masses between the eastern and the western Weddell Sea. In order to relate results obtained during the different time periods, empirical relationships are established between the length of the sea ice season, derived from the satellite passive microwave data and defined as the number of days per year with the sea ice concentration exceeding 15%, and (1) the annual mean ice draft and (2) the annual mean ice volume transport. By using these empirical relationships, estimates of annual mean ice drafts and ice volume transports are derived at all mooring sites for the period February 1979 through February 1999. Wind and current force a westward ice transport in the coastal areas of the eastern Weddell Sea and a northward ice transport in the west. During the 2-year period 1991/1992 the mean ice volume export from the Weddell Sea is $(50 \pm 19) \times 10^3$ m^3 s^{-1}. This freshwater export is representative for a longer-term (20-year) mean and exceeds the average amount of freshwater gained by precipitation and ice shelf melt by about 19×10^3 m^3 s^{-1}, yielding an upper bound for the formation rate of newly ventilated bottom water in the Weddell Sea of 2.6 Sv.

1. Introduction

Sea ice covers up to 10% of the total ocean surface and is one of the geophysical quantities most sensitive to climate variability [*Wadhams*, 1994]. Sea ice extent and concentration have been measured extensively by satellite remote sensing. In the Antarctic the sea ice area ranges from 4×10^6 km^2 in the southern summer to 20×10^6 km^2 in the southern winter [*Gloersen et al.*, 1992; *Heygster et al.*, 1996; *Zwally et al.*, 1983]. The pack ice of the Weddell Sea extends further north than anywhere else around the Antarctic continent, reaching a maximum distance of 2200 km from the coast at maximum extent. The sea ice thickness is, aside from sea ice concentration and extent, the fundamental variable to describe the influence of sea ice on the dynamic and thermodynamic interaction between the ocean and the atmosphere. Together with the ice drift it defines the mass flux of sea ice, which, in the Weddell Sea, is a major component of the freshwater budget.

The coldest and densest bottom water of the world ocean is formed in the Weddell Sea, which consequently represents a major ventilation area of the global ocean [*Brennecke*, 1921; *Deacon*, 1933; *Gordon*, 1971; *Mantyla and Reid*, 1983; *Mosby*, 1934; *Reid and Lynn*, 1971; *Wüst*, 1933]. Sea ice formation plays an important role in generating water masses dense enough to sink to the bottom of the Weddell Basin and thus in driving the thermohaline circulation. The significance of the influence of the sea ice cycle on the ocean is determined by the amount of freshwater lost during freezing and gained during melting. Owing to the sea ice drift, freezing and melting occur at different locations, and the destabilization of the water column during freezing is not necessarily balanced by the stabilization during melting. As a consequence, significant density contrasts may occur, leading to the formation of dense deep and bottom waters.

The objective of this study is to estimate the freshwater fluxes into and out of the southern Weddell Sea on the basis of long-term observations of sea ice thickness and ice drift. For this purpose, 13 upward look-

[1]Now at Institut für Meereskunde, Universität Kiel, Kiel, Germany.

Paper number 1999JC000027.
0148-0227/01/1999JC000027$09.00

ing sonars (ULS) were deployed in the Weddell Sea since 1990. They measure variations in ice draft, subsequently converted into ice thickness, throughout the year along two transects across the Weddell Sea. *Strass and Fahrbach* [1998] described the temporal and regional variation of sea ice draft and coverage obtained from the ULSs deployed in the central and western Weddell Sea between November 1990 and July 1994. The work presented here is based on their results and combines the 1990 to 1994 observations with new observations from April 1996 to April 1998 in the eastern Weddell Sea, along the meridian of Greenwich, for the estimation of the large-scale freshwater exchange between the sea ice and the ocean. Unlike sea ice thickness observations obtained by drilling, the ULS measurements provide observations of ice draft also during the southern winter, when vast regions of the Weddell Sea are inaccessible by ship. Furthermore, the ULS measurements are not limited to a subjectively defined range of ice thicknesses of floes which are thick enough to be walked on and thin enough to be drilled through.

The sea ice drift is determined by winds, currents, and the sea ice properties. In this study, ice drift is estimated from geostrophic winds for the period when ice draft measurements are available, using the empirical relationship determined by *Kottmeier and Sellmann* [1996]. On average, wind and current force the ice to move westward in the eastern Weddell Sea and northward in the west, producing a pattern of mean sea ice motion which reflects the cyclonic basin-wide circulation [*Hoeber*, 1991; *Kottmeier and Sellmann*, 1996; *Martinson and Wamser*, 1990; *Vihma and Launiainen*, 1993; *Vihma et al.*, 1995; *Wadhams et al.*, 1989]. The difference between ice import from the east and export in the west provides a freshwater exchange with the underlying southern Weddell Sea.

The next section will briefly describe the ULS array and the data processing procedures applied to the raw data to yield accurate measurements of ice draft. Mean ice drift and ice draft characteristics are described in sections 3 and 4. Ice draft is converted to ice thickness, and together with the ice drift, integrated ice and salt transports across the mooring transects are derived in section 5. In order to relate results obtained during different observation periods, empirical relationships are established between the length of the sea ice season, derived from the satellite passive microwave data and defined as the number of days per year with the sea ice concentration exceeding 15% and (1) the annual mean ice draft and (2) the annual mean ice volume transport (section 6). By using these empirical relationships, annual mean ice drafts and ice volume transports are derived at all mooring sites for the 20-year period February 1979 to February 1999 and are analyzed for interannual variations. The significance of the estimated transports for the freshwater budget in the Weddell Sea is discussed in section 7.

2. Observations

Ice draft is measured with moored upward looking sonars since 1990 along two transects across the Weddell Sea (Figure 1). Six ULSs were deployed between 1990 and 1994 (Table 1) on the transect extending from the tip of the Antarctic Peninsula to Kapp Norvegia, covering the flow into and out of the southern Weddell Sea [*Strass and Fahrbach*, 1998]. Along this transect the westernmost instrument and one additional instrument even further to the west were redeployed in 1996 for a time period of 2 years. Six ULSs were deployed in 1996 on the transect extending from the Antarctic continent northward along the Greenwich meridian, covering the exchange of water masses between the eastern and the western Weddell Sea. These six instruments are still operating after redeployment.

The ULSs, manufactured by the Christian-Michelsen Research Institute in Bergen, Norway [*Johannessen*, 1995; *Lothe*, 1997], are mounted to the top of moorings, 125 to 175 m below the sea surface (Figure 2, Table 2). They transmit a burst of four 300-kHz sound pulses at the specified sample interval from their depth of deployment to the surface and measure the time until the return of the echo. The distance between the instrument and the reflecting target is derived from the sound pulse travel time, under consideration of the vertical sound velocity distribution above the ULS. The vertical sound velocity profile and its variation in time is obtained with the aid of a dynamic-thermodynamic sea ice mixed layer model for the Weddell Sea [*Timmermann et al.*, 1999], adjusted to the temperature record at the instrument and the salinity and temperature profiles measured during the deployment and recovery cruises. Using this sound velocity model, the sound pulse travel times are converted to distances. The ULSs are further equipped to measure pressure, water temperature, echo amplitude, and instrument tilt. The depth of the instrument is derived after adjusting the pressure sensor records for air pressure variations, using the analyses of the European Centre for Medium-Range Weather Forecasts (ECMWF) near the mooring sites interpolated to the sample interval of the ULS measurements. Subtraction of the echo-derived range from the instrument's depth yields the depth of the sound reflecting target, i.e., the ice draft when the echo originates from a water-ice interface. The rms distance error of the empirical sound velocity model is estimated by comparison with sound velocity profiles obtained from conductivity-temperature-depth (CTD) casts to 0.06 m. In combination with inaccuracies of the surface pressure fields the rms distance error increases to 0.19 m. This error is reduced to less than 0.03 m after final adjustment of the surface level based on drafts identified as open water [*Strass*, 1998].

The opening angle of the acoustic beam is 2°, which together with an average ULS deployment depth of 150 m results in a footprint diameter of approximately

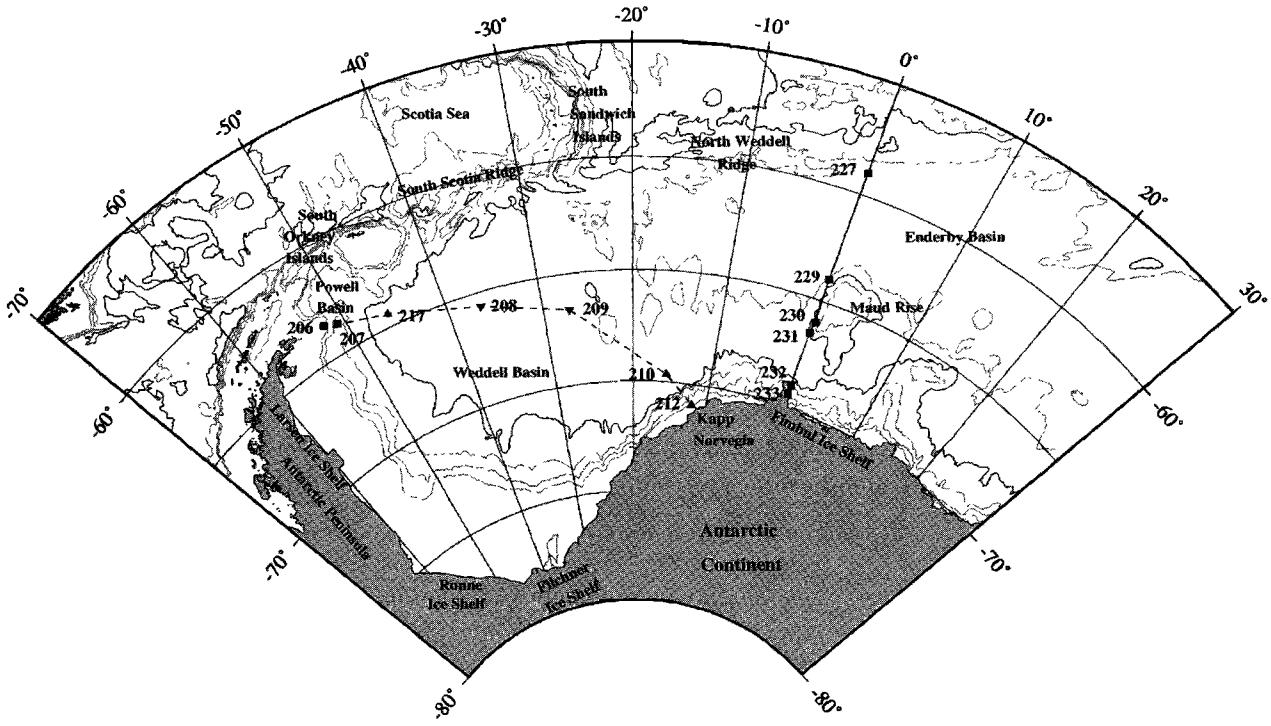

Figure 1. Map of upward looking sonar moorings maintained by the Alfred Wegener Institute since 1990 in the Weddell Sea. Moorings represented by upright triangles were deployed from November 1990 to January 1993, those represented by inverted triangles were deployed from January 1993 to March 1995, and those represented by squares were deployed in February 1996 and are still operating. The periods covered by measurements at the mooring locations are given in Table 1. Dashed lines represent conductivity-temperature-depth transects, completed four times since 1989.

10 m. The associated footprint error depends on the roughness and slope of the ice bottom, the ice concentration, and how the ice field is broken up (i.e., if there are small openings in the ice that the ULS fails to detect). Best results are obtained in the idealistic case when ice floes are large and flat. Since this is not always the case, the bias which is likely to result from the effect of beam spreading is determined from horizontal drill profiles in the Weddell Sea and is subsequently removed from the ice draft measurements (see *Strass* [1998] for details). After processing, the error in the ice draft measurement amounts to 0.04 m [*Strass*, 1998]. Detailed information on the data processing procedure and the error estimation are found in the work of *Strass* [1998] and *Strass and Fahrbach* [1998].

Ice draft (d) represents only the submerged portion of an ice floe. Ice thickness (z) is the sum of draft and freeboard of an ice floe (Figure 2). Ice draft is converted to ice thickness by using an empirical relationship established from thickness drillings in the Weddell Sea (section 5). Adopting the notation from *Strass and Fahrbach* [1998], mean ice draft ($\overline{d}$) represents the sum of all draft measurements of ice divided by the number of data cycles identified as ice, during the given time period. In contrast, effective ice draft ($\overline{d}_{\text{eff}}$) represents the sum of all draft measurements of ice divided by the total number of data cycles, including both ice and water, during the given time period. In other words, effective ice draft represents the mean ice draft including observations of zero ice thickness (i.e., open water). It follows that effective ice draft contains indirect information about the sea ice coverage. By definition, $\overline{d}_{\text{eff}} \leq \overline{d}$, and these two quantities are equal only if there are no ice-free periods. In this paper, whenever mean quantities are considered, effective ice draft is used, since it enters the transport equations in sections 5 and 6. The standard error of the mean is calculated as the ratio of the standard deviation to the square root of the number of independent observations in the particular time interval. The number of independent observations is estimated by relating the product of the sampling rate and surface window to the ice drift speed (see section 3). The statistical error is in addition to the measurement uncertainty of 0.04 m indicated above. The ice draft mode is the most frequent draft, defined as the maximum of the probability density function. Ice coverage represents the fraction of time that ice is present at the ULS mooring position during a given period. This quantity can be directly compared with the sea ice concentration obtained from satellite imagery, if the ice field passes the ULS at a constant speed.

The local measurements of sea ice coverage at the

Table 1. Alfred Wegener Institute ULS Mooring Locations and Measurement Periods in the Weddell Sea[a]

Mooring	SN	Model	Version	Latitude	Longitude	WD	ID	SI	Start	End
206-4	09	ES-300 V	3.0	63°29.6'S	52°06.1'W	960	157	15	May 8, 1996	Jan. 8, 1998
207-2	06	ES-300 V	1.0	63°45.1'S	50°54.3'W	2461	125	8	Nov. 22, 1990	Nov. 26, 1992
207-3[b]	27	ES-300 V	1.0	63°45.0'S	50°54.3'W	2498	...	...	...	...
207-4	08	ES-300 V	3.0	63°43.3'S	50°49.2'W	2510	174	15	April 27, 1996	Nov. 7, 1997
208-2[c]	08	ES-300 V	1.0	65°38.1'S	36°30.0'W	4710	...	...	...	...
208-3	24	ES-300 V	1.0	65°37.7'S	36°29.4'W	4766	150	8	Jan. 4, 1993	July 25, 1994
209-2[b]	11	ES-300 V	1.0	66°37.3'S	27°07.0'W	4860	...	...	...	...
209-3	25	ES-300 V	1.0	66°37.4'S	27°07.2'W	4860	132	8	Dec. 31, 1992	Nov. 10, 1993
210-2	07	ES-300 V	1.0	69°39.6'S	15°42.9'W	4750	125	8	Dec. 11, 1990	Dec. 16, 1992
210-3[b]	28	ES-300 V	1.0	69°38.5'S	15°43.6'W	4750	...	...	...	...
212-2	09	ES-300 V	1.0	70°54.7'S	11°57.8'W	1550	125	8	Dec. 14, 1990	Dec. 18, 1992
212-3[b]	23	ES-300 V	1.0	70°54.6'S	11°57.9'W	1540	...	...	...	...
217-1	10	ES-300 V	1.0	64°25.1'S	45°51.0'W	4390	125	8	Nov. 24, 1990	Nov. 26, 1992
217-2[c]	26	ES-300 V	1.0	64°25.0'S	45°49.8'W	4420	...	...	...	...
227-3	10	ES-300 V	1.0	59°01.8'S	00°00.1'E	4605	156	8	April 4, 1996	Jan. 10, 1997
227-4	37	ES-300 VI	4.0	59°01.8'S	00°00.9'W	4600	145	3	Jan. 9, 1997	April 11, 1998
229-1	07	ES-300 V	3.0	64°00.0'S	00°00.0'E	5186	165	15	April 18, 1996	Dec. 24, 1997
230-1[c]	25	ES-300 VI	4.0	66°00.2'S	00°09.5'E	3450	...	...	...	...
231-1	26	ES-300 V	3.0	67°00.0'S	00°00.4'W	4510	160	15	April 12, 1996	Dec. 27, 1997
232-1	24	ES-300 V	3.0	69°00.0'S	00°00.0'E	3361	147	15	April 21, 1996	Feb. 16, 1997
232-2[b]	35	ES-300 VI	4.0	69°00.0'S	00°00.0'E	3361	...	...	...	...
233-1[b]	06	ES-300 V	3.0	69°24.2'S	00°00.7'E	2000	...	...	...	...
233-2	34	ES-300 VI	4.0	69°24.0'S	00°00.0'E	1960	154	3	Feb. 16, 1997	March 12, 1998

[a]SN, serial number; WD, water depth in meters; ID, instrument depth in meters; SI, sampling interval in minutes.
[b]Instrument lost.
[c]Instrument failure.

mooring sites are supplemented by basin-wide observations derived from Scanning Multichannel Microwave Radiometer (SMMR) and Special Sensor Microwave Imager (SSM/I) data, which have been daily archived and processed since the late 1970s as part of the Project of Estimation of Long-Term Variability in Ice Concentration (PELICON) [*Heygster et al.*, 1996]. The comparison of the SMMR (1979-1987) and SSM/I (1987-1999) data sets during a 6-week period of overlap in July and August 1987 indicates that the sea ice concentrations and extents obtained from the two instruments differ only by a few percent [*Parkinson*, 1998]. Since in this paper we are not calculating long-term trends, our results are qualitatively not affected by combining the data sets from the two instruments. The spatial resolution of the satellite passive microwave data is 25 by 25 km. The estimates are accurate within 10% [*Cavalieri*, 1992; *Comiso et al.*, 1992].

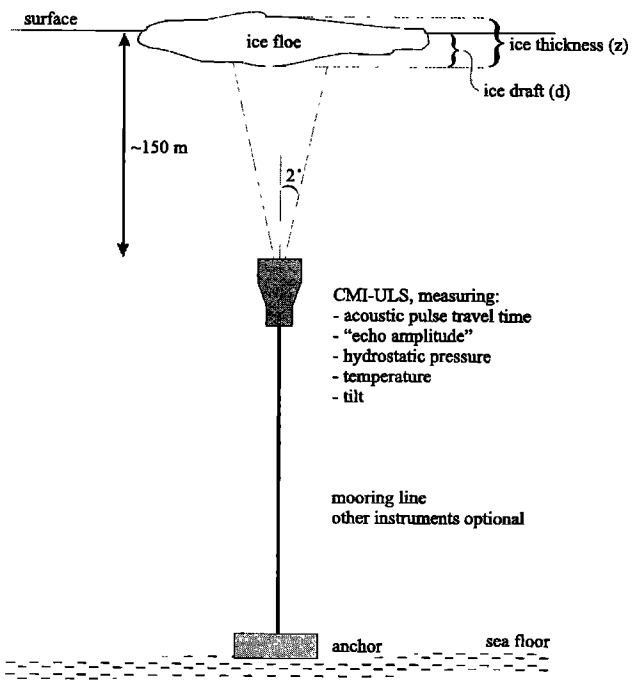

Figure 2. Schematic representation of a ULS deployment.

Conductivity-temperature-depth surveys were conducted during the deployment and recovery cruises with a CTD sonde connected to a General Oceanics' rosette water sampler with 24 12-L bottles. The analyses of the CTD data are described in detail by *Schröder and Fahrbach* [1999]. Hydrographic transects across the central and western Weddell Sea, extending from the tip of the Antarctic Peninsula to Kapp Norvegia, and along the Greenwich meridian were completed four times since 1989 [*Augstein et al.*, 1991; *Bathmann et al.*, 1992, 1994; *Fahrbach and Gerdes*, 1997; *Fahrbach*, 1999; *Lemke*, 1994]. Meteorological parameters near the mooring sites are available from the analyses of the European Centre for Medium-Range Weather Forecasts. The ECMWF analyses include data from manned and unmanned stations by the ECMWF assimilation procedure [*European Centre for Medium-Range Weather Forecasts*, 1992]. The spatial resolution of the ECMWF

Table 2. Technical Specification of the ULS

Parameter	Specification	Comment
Acoustic frequency	300 kHz	corresponds to a wavelength of 0.5 cm
Pulse width	66 ms	
Resolution of sound pulse travel time	model V: 13 ms	corresponds to an acoustic distance of 1 cm
	higher models: 814 ns	corresponds to an acoustic distance of 0.6 cm
Opening angle of acoustic beam	2°	corresponds to a surface window 10 m in diameter
Resolution of pressure	5 hPa	
Resolution of tilt	1°	
Resolution of temperature	0.1 K	
Operational depth range	10-190 m	
Maximum permissible depth	400 m	

data is 1.125° for both latitude and longitude and the time resolution is 6 hours. Our subsequent analyses are all based on 6-hourly averages of the original measurements. The 6-hour time interval matches the temporal resolution of the ECMWF air pressure fields from which the geostrophic winds are derived. Goodness-of-fit measures for all regression analyses presented in this paper are given in terms of r^2, which represents the proportion of the variation of the predictand that is accounted for by the regression. For a perfect regression, $r^2 = 1$.

3. Ice Drift

In the Weddell Sea, ice drift is closely linked to the geostrophic wind [*Kottmeier et al.*, 1992; *Kottmeier and Sellmann*, 1996; *Thorndike and Colony*, 1982]. Ice drift speeds at the mooring sites are estimated from the ECMWF geostrophic winds, using the empirical relationship determined by *Kottmeier and Sellmann* [1996]. They applied a complex linear model of ice drift [*Thorndike and Colony*, 1982],

$$\mathbf{D} = \overline{\mathbf{C_g}} + \overline{\mathbf{A}}\,\mathbf{V_g} + \epsilon, \qquad (1)$$

to study the forcing of Weddell Sea ice motion. In equation (1), $\mathbf{D}$ is the ice drift vector; $\mathbf{V_g}$ represents the geostrophic wind vector; $\overline{\mathbf{C_g}}$ is the mean, not the wind-correlated part, of the ice motion, which includes mean effects of ocean currents, internal stresses, and ocean surface tilt; $\overline{\mathbf{A}}$ is a complex multiplier linearly relating ice drift fluctuations to geostrophic wind variations; and ϵ is the complex residual representing ice drift fluctuations which are neither constant nor linearly related to winds. *Kottmeier and Sellmann* [1996] combined observations of sea ice drift, using data from sea ice buoys, and geostrophic winds, derived after matching the surface pressure fields of the ECMWF with the buoy pressure data, and used equation (1) as a regression equation to calculate the regional distribution of the optimum parameters $\overline{\mathbf{C_g}}$ and $\overline{\mathbf{A}}$ for the Weddell Sea. Their linear model accounts for less than 50% of the ice drift variance in the southwestern Weddell Sea but for up to 75% of the total variance in the other areas of the Weddell Sea, suggesting that the linear model is a reasonable estimator of ice motion in large parts of the basin and at our measurement sites.

In this study, we use *Kottmeier and Sellmann*'s [1996] parameters $\overline{\mathbf{C_g}}$ and $\overline{\mathbf{A}}$ and combine them with observations of geostrophic wind for the period of our ice draft measurements to obtain the ice drift at the mooring sites. The geostrophic wind components u_g (positive eastward) and v_g (positive northward) for each moor-

Table 3. Modulus and Phase of the Complex Multiplier $\overline{\mathbf{A}}$ and the x and y Components of $\overline{\mathbf{C_g}}$ at the Mooring Positions

Mooring	Latitude	Longitude	Modulus A,[a] %	Phase A,[b] deg	C_x, m s^{-1}	C_y, m s^{-1}
206	63°29.6'S	52°06.1'W	1.20	5.0	0.010	0.040
207	63°43.3'S	50°49.2'W	1.20	5.0	0.010	0.040
217	64°25.1'S	45°51.0'W	1.30	5.0	-0.005	0.020
208	65°37.7'S	36°29.4'W	1.30	6.2	0.000	0.015
209	66°37.4'S	27°07.2'W	1.35	3.5	-0.005	0.005
210	69°38.5'S	15°43.6'W	1.55	5.0	-0.020	0.000
212	70°54.6'S	11°57.9'W	1.55	4.8	-0.030	-0.010
227	59°01.8'S	00°00.9'W	1.70	0.0	0.010	0.000
229	64°00.0'S	00°00.0'W	1.65	-0.4	0.005	0.005
231	67°00.0'S	00°00.4'W	1.60	-1.0	0.000	0.005
232	69°00.0'S	00°00.0'W	1.50	-1.0	-0.020	0.000
233	69°24.0'S	00°00.0'W	1.50	-0.5	-0.030	0.000

[a]The modulus of the complex multiplier $\overline{\mathbf{A}}$ relates the ice drift speed to the geostrophic wind speed.
[b]The phase of the complex multiplier $\overline{\mathbf{A}}$ represents the angle between ice motion and geostrophic wind.

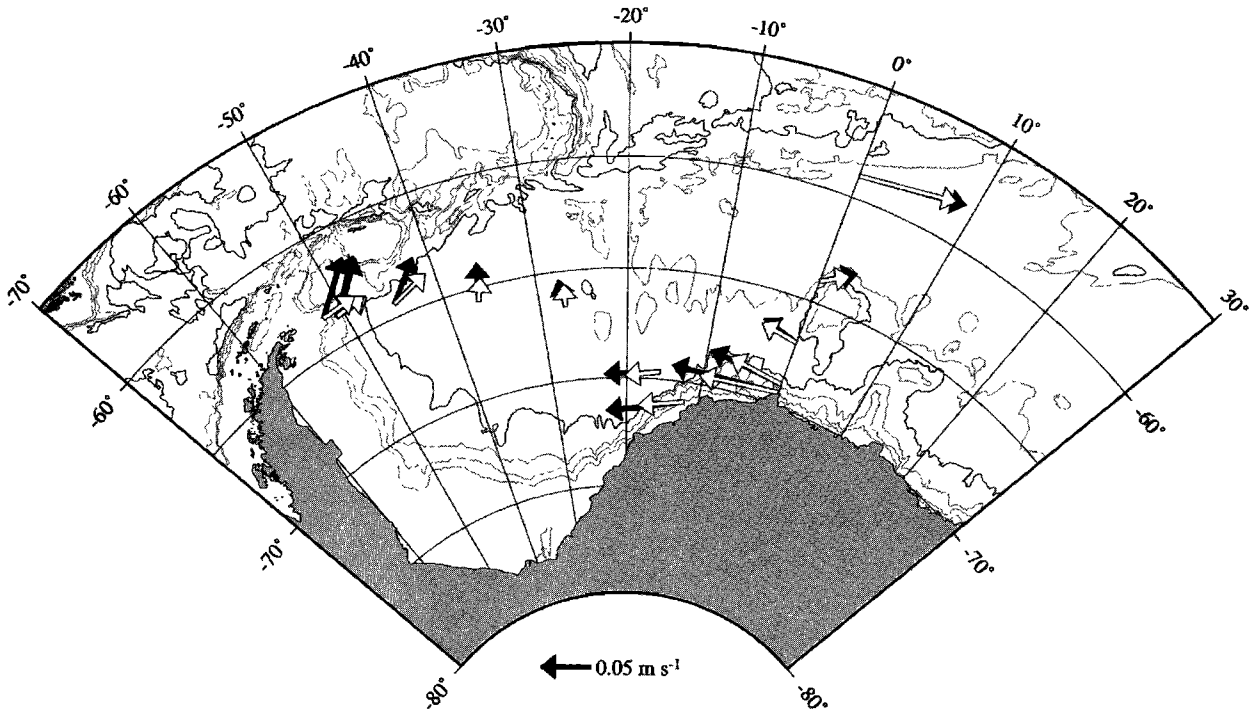

Figure 3. Mean ice drift in meters per second at mooring locations. The ice drift is estimated according to equation (1) and averaged over the ULS deployment periods. Ice drift fluctuations which are neither constant nor linearly related to winds are ignored ($\epsilon = 0$) (solid arrows). Open arrows show the ice drift when the mean, not wind-correlated part, of the ice motion, which includes mean effects of ocean currents, internal stresses, and ocean surface tilt, is zero ($\overline{C_g} = 0$).

ing position are calculated from the 6-hour surface air pressure analyses of the ECMWF. The constants $\overline{\mathbf{C_g}}$ and $\overline{\mathbf{A}}$ are extracted at the mooring positions from the composite spatial distributions (Table 3, and *Kottmeier and Sellmann* [1996, Figures 14-16]).

Wind and current produce a pattern of mean sea ice motion which reflects the basin-wide circulation of the cyclonic Weddell Gyre. During the time of mooring deployment (see Table 1) the mean ice drift at the mooring sites is westward in the southern Weddell Sea, northeastward in the western Weddell Sea near the tip of the Antarctic Peninsula, and eastward in the northern Weddell Sea (Figure 3). Ice drift speeds are largest near the gyre's edges and smallest in the center. The largest mean ice drift speeds (0.11 m s^{-1}) occur in the northern Weddell Sea at ALfred Wegener Institute (AWI) mooring AWI-227, a region of strong westerly winds, and in the southeastern Weddell Sea at AWI-233, a region of prevailing easterly winds and strong westward boundary currents. About 500 km to the west of AWI-233, at AWI-212, easterly winds and westward currents produce an offshore drift component, and the mean ice drift is reduced (0.08 m s^{-1}). At the western boundary, off the tip of the Antarctic Peninsula, wind (eastward) and current (northward) are directed perpendicular to each other, resulting in a mean ice drift smaller than that at the eastern boundary (0.06 m s^{-1} at AWI-206 and AWI-207). The mean ice drift is smallest in the central Weddell Sea (0.03 m s^{-1} at AWI-209; 0.04 m s^{-1} at AWI-208, AWI-229, and AWI-231), a region where winds and currents are highly variable. The standard errors of the means are less than 10% of the mean values.

4. Effective Draft and Ice Draft Mode

Mean effective drafts in the western Weddell Sea increase from the center of the gyre toward the boundaries (Figure 4a (left panel), Table 4). In the center of the gyre, effective drafts averaged over the 2-year period 1993/1994 are 0.59 m at AWI-209 and 0.92 m at AWI-208. Near the boundaries, effective drafts averaged over the 2-year period 1991/1992 increase toward the boundary from 0.80 m (AWI-210) to 1.90 m (AWI-212) in the southeast and from 1.41 m (AWI-217) to 2.20 m (AWI-207) in the west. During the 2-year period 1996/1997 the effective draft at AWI-207 is 1.40 m, 0.8 m smaller than that in 1991 and 1992. The ice draft mode changes across the gyre inversely to the mean (Figure 4b). It is highest in the center of the gyre (0.8 m at AWI-209) and lowest in the boundary regions (0.2 m on both sides). In the northwestern Weddell Sea near the Antarctic Peninsula the probability density function of ice draft is bimodal with a secondary, broader peak of comparable magnitude centered around 1.0 m (Table 4). In the eastern Weddell Sea, effective drafts averaged

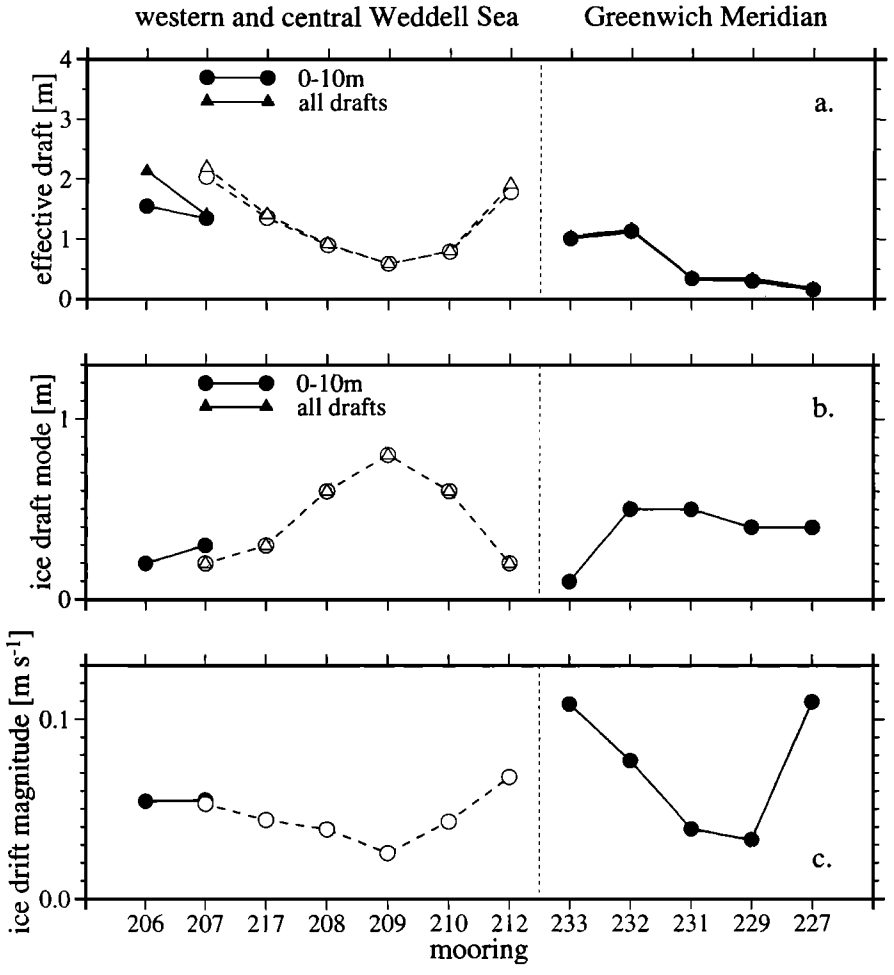

Figure 4. Horizontal profile of (a) the effective draft, $\overline{d}_{\text{eff}}$, and (b) the ice draft mode, crossing the Weddell Sea along the western transect from northwest to southeast and along the eastern transect from south to north. (c) Magnitude of the mean ice drift component normal to the transects, $\overline{D}_{\perp}$. Open symbols and dashed lines refer to averaged quantities of the 1991/1992 and 1993/1994 deployments; solid symbols and lines refer to averaged quantities of the 1996/1997 deployment.

over the 2-year period 1996/1997 increase from north to south (Figure 4a (right panel)). The effective draft increases from 0.18 m at AWI-227 to 1.16 m at AWI-232 and 1.03 m at AWI-233. The mean effective draft at AWI-232 (AWI-233) is 0.75 m (0.88 m) smaller than the 1991/1992 mean at AWI-212, about 500 km to the west. This difference is of the same order of magnitude as the difference between the 1991/1992 and 1996/1997 mean effective drafts at AWI-207 in the western Weddell Sea (see above). The ice draft mode (Figure 4b) is lowest near the Antarctic continent (0.1 m at AWI-233). Away from the coast the mode is rather constant with values ranging from 0.4 m to 0.5 m.

Less than 2.5% of the measured ice drafts exceed 10 m (Table 4). Most of the ice formed in this area reaches an age of less than 2 years before it leaves the Weddell Sea with the gyre circulation and eventually melts north of the Weddell Front. Ice drafts larger than 10 m can be sea ice ridges, growlers, or icebergs. Taking 10 m as a threshold, the 2-year averages of effective draft in the boundary regions are $\leq$0.16 m smaller than those obtained from the full range (Table 4). At AWI-206, however, the mooring closest to the Antarctic Peninsula, the difference is larger (0.59 m). This is due to the frequent occurrence of both large-pressure ridges and icebergs, as observed during the cruises in this area. Away from the boundaries the 2-year averages of drafts less than 10 m are $\leq$0.02 m smaller than those obtained from the full range.

Prevailing easterly winds off Kapp Norvegia in the southeastern Weddell Sea have a slight offshore component. The wind stress acting on the ice surface causes the ice cover to open up and to form leads or polynyas in which new ice can be continuously formed. Frequent new ice formation near the coast leads to low ice draft modes ($\leq$0.2 m) (Figure 4, Table 4). When easterly winds weaken, or even reverse, the combined effect of winds and currents with the presence of the coast en-

Table 4. Effective Ice Draft, Ice Draft Mode, Ice Coverage, and Classification by Draft Ranges at the ULS Positions

Mooring	Time Period	Effective Draft,[a] m		Mode,[b] m	Coverage, %	Classification by Draft Ranges, %			
		All Drafts	Drafts ≤10 m			0-0.5 m	0.51-1.5 m	1.51-10 m	>10 m
206	1996 - 1997	2.14 ± 0.04	1.55 ± 0.02	0.2 (1.1)	73.7	15.5	25.6	56.8	2.3
207	1996 - 1997	1.40 ± 0.02	1.35 ± 0.02	0.3 (1.0)	72.1	19.2	33.6	46.8	0.4
207	1991 - 1992	2.20 ± 0.03	2.04 ± 0.02	0.2 (1.1)	80.0	14.2	24.8	59.2	1.8
217	1991 - 1992	1.41 ± 0.02	1.36 ± 0.02	0.3 (0.6)	82.2	23.6	37.0	39.0	0.4
208	1993 - 1994	0.92 ± 0.01	0.90 ± 0.01	0.6	84.1	27.7	52.4	19.8	0.1
209	1993 - 1994	0.59 ± 0.01	0.59 ± 0.01	0.8	75.8	33.2	57.9	8.9	<0.1
210	1991 - 1992	0.80 ± 0.01	0.79 ± 0.01	0.6	77.3	33.5	47.3	19.1	0.1
212	1991 - 1992	1.91 ± 0.03	1.78 ± 0.02	0.2	85.5	27.3	24.7	46.8	1.2
233	1996 - 1997	1.03 ± 0.03	1.01 ± 0.02	0.1 (0.5)	65.3	31.3	39.1	29.0	0.6
232	1996 - 1997	1.16 ± 0.03	1.13 ± 0.02	0.5	80.1	25.6	43.6	30.4	0.4
231	1996 - 1997	0.36 ± 0.01	0.34 ± 0.01	0.5	60.6	58.3	36.1	5.5	0.1
229	1996 - 1997	0.33 ± 0.01	0.30 ± 0.01	0.4	53.9	62.5	30.5	6.9	0.1
227	1996 - 1997	0.18 ± 0.01	0.16 ± 0.01	0.4	31.0	63.3	35.9	0.8	<0.1

[a]Effective draft, $\overline{d}_{\text{eff}}$, is the sum of all draft measurements of ice, divided by the number of data cycles identified as ice and water. The (±) values in columns 3 and 4 represent the standard errors of the means. This error is in addition to the measurement uncertainty of 0.04 m.
[b]Secondary maxima of the probability density function are listed in parentheses.

hances the formation of ridges, and particularly thick ice occurs. The ridging during periods of higher winds leads to a close correlation between ice thickness and wind speed (not shown).

The drift of sea ice buoys deployed in this region suggests that the ice tends to follow the local isobath [*Harder and Fischer*, 1999; *Kottmeier et al.*, 1992]. Near the coast, the gyre circulation carries ice from the southeastern Weddell Sea into the southern Weddell Sea and then northward up the eastern side of the Antarctic Peninsula. The mean effective draft in the western Weddell Sea exceeds the mean in the southeast by more than 0.3 m (Figure 4, Table 4). *Strass and Fahrbach* [1998] show that during circulation with the Weddell Gyre mainly ice with a draft less than 1 m is transformed into thicker ice. Their results indicate that the major transformation occurs from drafts of 0.2 m to drafts of 1.2 m. Off the tip of the Antarctic Peninsula westerly winds prevail. The offshore winds frequently create open water areas where new ice is formed and subsequently discharged into the Antarctic Circumpolar Current, leading to the low ice draft modes observed here (<0.3 m). The secondary maximum in the modal ice draft at about 1.0 m (Table 4) results from the advection of deformed ice (see *Strass and Fahrbach* [1998] for details).

5. Ice and Salt Transports

The ice drift accomplishes a large-scale transport of freshwater, and the saline brine rejected during freezing contributes substantially to the formation of dense deep and bottom waters. To quantify the freshwater exchange between the sea ice and the ocean, 6-hourly averaged time series of effective draft and ice drift, measured during three 2-year periods in 1991/1992, 1993/1994, and 1996/1997, are combined for estimation of the ice and salt transports in the western and eastern Weddell Sea. Ice transports are calculated in two ways. First, all ice drafts are included in the analysis; second, ice drafts larger than 10 m, representing either sea ice ridges, growlers, or icebergs (see section 4), are excluded from the calculations. Except at AWI-206, the resulting transports are not significantly different.

Ice draft is converted to ice thickness by using an empirical relationship established from thickness drillings in the Weddell Sea [*Eicken et al.*, 1994; *Lange and Eicken*, 1991; *Wadhams et al.*, 1987] (Figure 5). The thickness drillings yield estimates of the draft of an ice floe, its thickness, and the snow depth on top of it. For the establishment of the empirical relationship, only the ice thickness data are considered. The effect of the snow cover is discussed at the end of this section. On the basis of these observations, ice draft d and ice thickness z are approximately linearly related according to

$$z = 0.028 + 1.012\,d, \tag{2}$$

with $r^2 = 0.99$.

The salinity of sea ice decreases with increasing ice thickness. This decrease is due to the continuing desalination after the ice is deformed, providing a salt flux to the ocean over a period of time longer than the initial growth phase. To describe the salinity of sea ice as a continuous function of ice thickness, a line is fitted to the salinity measurements obtained from ice core drillings in the Weddell Sea [*Eicken et al.*, 1991; *Eicken*, 1992, 1998] (Figure 6). For ice thicknesses ≤1.85 m a linear relationship between ice thickness and salinity according to

$$S = 7.286 - 1.776\,z \qquad z \leq 1.85 \text{ m} \tag{3a}$$

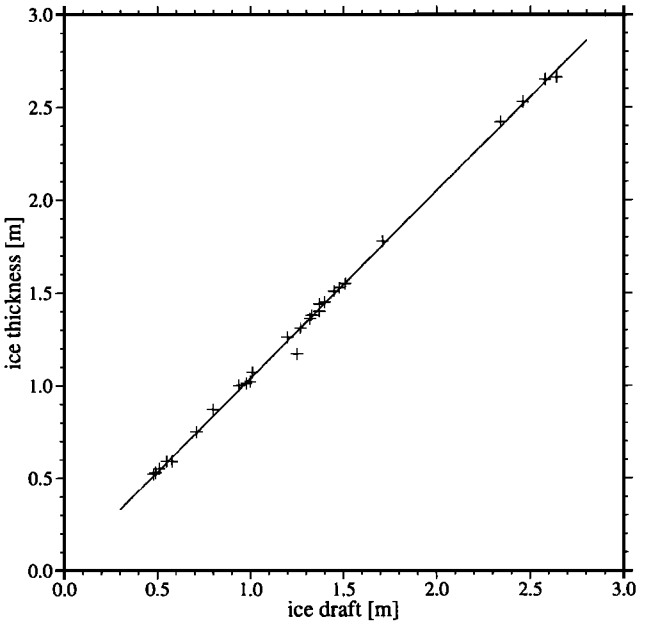

Figure 5. Empirical relationship between ice draft d and ice thickness z established from thickness drillings in the Weddell Sea (solid line and plus signs) [after *Eicken et al.*, 1994; *Lange and Eicken*, 1991; *Wadhams et al.*, 1987]. On the basis of these observations, ice draft and ice thickness are approximately linearly related according to equation (2).

($r^2 = 0.39$) is assumed. For thicker floes a constant salinity of 4.0 is assumed (H. Eicken, personal communication, 1998):

$$S = 4.0 \qquad z > 1.85 \text{ m}. \tag{3b}$$

The ice and salt transports at the mooring sites are in the direction of the ice drift (see Figure 3). To estimate the net transport across transects, the transports at each mooring site are projected onto the component normal to the respective transect (represented by the perpendicular symbol) and are then linearly interpolated across the transect. Integrated transports are estimated on the basis of the horizontally interpolated values. The transports vanish at the coast and on the Greenwich meridian at 55°00'S, the latitude of the average northernmost extent of the ice edge. Ice drift and ice transport across the western transect also vanish in the center of the gyre at 22°10'W, 67°18'S [*Kottmeier and Sellmann*, 1996]. West of this point the transect is oriented 107° relative to north; east of this point it is oriented 135° relative to north. Negative values represent transports to the west or southwest, i.e., into the central Weddell Sea. Positive values represent transports to the east or northeast, i.e., out of the central Weddell Sea.

The ice volume transport at the mooring sites normal to the transect, $\Phi_\perp$, is estimated according to

$$\Phi_\perp = D_\perp z \tag{4}$$

(per unit width), where $D_\perp$ is the ice drift component normal to the transect and z is the ice thickness. Because of small variations in the density of Antarctic sea ice, ice volume transport can be translated directly into ice mass transport with little error by using an average density $\rho_i = 910$ kg m^{-3} (H. Eicken, personal communication, 1998). Associated with the transport of ice volume is a transport of salt, $M_{\perp s}$, estimated by multiplying the volume transport with the mean salinity of sea ice, S, and the sea ice density, ρ_i,

$$M_{\perp s} = \Phi_\perp \rho_i S \tag{5}$$

(per unit width). The amount of salt released to the ocean during sea ice formation is estimated according to

$$M_{\perp s_{34.4}} = \Phi_\perp \rho_i (S - 34.4) \tag{6}$$

(per unit width), where 34.4 is the reference salinity of Winter Water from which most of the sea ice is formed.

First, we consider the case when all ice drafts are included in the analysis (Table 5). Across the eastern transect, wind and current force an average eastward ice volume transport of $(17 \pm 4) \times 10^3$ m^3 s^{-1} in the north and an average westward ice volume transport of $(25 \pm 3) \times 10^3$ m^3 s^{-1} in the south (Figure 7, Table 6). The 1996/1997 westward ice transport at the Greenwich meridian agrees, within the error bars, with the 1991/1992 southwestward transport off Kapp Norvegia, about 500 km to the west. Across the line extending

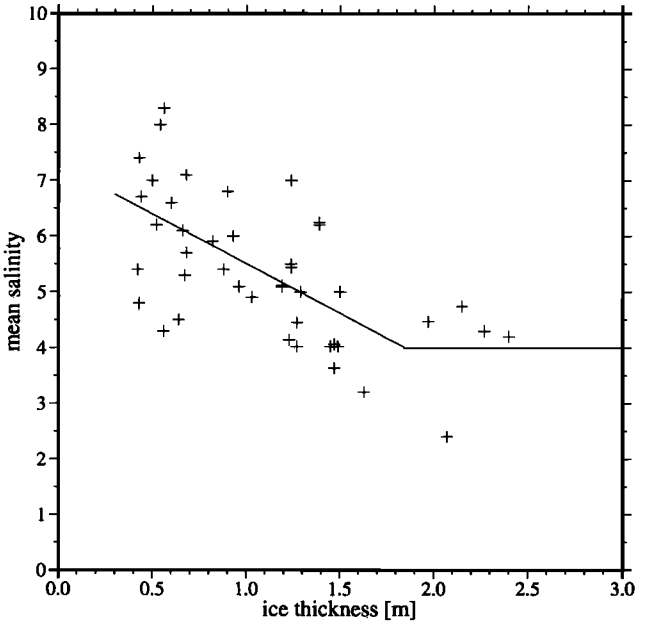

Figure 6. Empirical relationship between ice thickness z and mean salinity S of the ice floe established from ice core drillings in the Weddell Sea [after *Eicken et al.*, 1991; *Eicken*, 1992, 1998]. For ice thicknesses $\leq$1.85 m a linear relationship between ice thickness and mean salinity according to equation (3) is assumed. For thicker floes a constant mean salinity of 4.0 is assumed.

Table 5. Mean Ice and Salt Transports Normal to the Transects[a]

Mooring	Time Period	Ice Volume Transport, $\times 10^{-3}$ m^3 s^{-1}		Ice Mass Transport, kg s^{-1}		Salt Mass Transport, $\times 10^{-2}$ kg s^{-1}		$Salt_{34.4}$ Mass Transport, $\times 10^{-1}$ kg s^{-1}	
		All Drafts	Drafts $\leq$10 m	All Drafts	Drafts $\leq$10 m	All Drafts	Drafts $\leq$10 m	All Drafts	Drafts $\leq$10 m
206	1996-1997	118 ± 21	92 ± 17	107 ± 19	84 ± 15	45 ± 19	35 ± 11	-32 ± 7	-25 ± 5
207	1996-1997	85 ± 15	82 ± 15	77 ± 14	74 ± 13	33 ± 10	33 ± 9	-23 ± 5	-22 ± 4
				Western Transect					
207	1991-1992	126 ± 24	117 ± 22	115 ± 21	107 ± 20	48 ± 22	44 ± 19	-35 ± 8	-32 ± 7
217	1991-1992	68 ± 15	65 ± 15	62 ± 14	59 ± 13	28 ± 10	27 ± 10	-18 ± 5	-18 ± 4
208	1993-1994	40 ± 10	40 ± 10	36 ± 9	36 ± 9	18 ± 6	18 ± 6	-11 ± 3	-11 ± 3
209	1993-1994	21 ± 8	21 ± 8	19 ± 7	19 ± 7	11 ± 5	11 ± 5	-5 ± 2	-5 ± 2
210	1991-1992	-38 ± 9	-38 ± 9	-35 ± 8	-34 ± 8	-18 ± 5	-18 ± 5	10 ± 2	10 ± 2
212	1991-1992	-149 ± 22	-138 ± 20	-135 ± 20	-126 ± 19	-57 ± 18	-54 ± 16	41 ± 7	38 ± 6
				Eastern Transect					
233	1996-1997	-125 ± 12	-123 ± 12	-113 ± 11	-112 ± 11	-53 ± 7	-52 ± 7	34 ± 4	33 ± 3
232	1996-1997	-81 ± 11	-80 ± 11	-73 ± 10	-73 ± 10	-37 ± 7	-37 ± 7	22 ± 3	21 ± 3
231	1996-1997	-18 ± 5	-18 ± 5	-16 ± 4	-16 ± 4	-10 ± 3	-10 ± 3	5 ± 1	5 ± 1
229	1996-1997	10 ± 3	9 ± 3	9 ± 3	8 ± 3	6 ± 2	5 ± 2	-3 ± 1	-2 ± 1
227	1996-1997	26 ± 5	23 ± 5	24 ± 5	21 ± 4	15 ± 3	14 ± 3	-7 ± 1	-6 ± 1

[a]Negative volume and mass transports are directed to the west or southwest into the central Weddell Sea. Positive volume and mass transports are directed to the east or northeast out of the central Weddell Sea. The $salt_{34.4}$ mass transport is identical to $M_{S_{34.4}}$ in equation (6) and represents the salt mass transport relative to the salinity of Winter Water. By definition, the sign of $M_{S_{34.4}}$ is opposite to that of the salt mass transport (M_S).

from the tip of the Antarctic Peninsula to Kapp Norvegia, wind and current force an average southwestward ice volume transport of $(28 \pm 5) \times 10^3$ m^3 s^{-1} in the east into the Weddell Sea and a northward ice volume transport of $(78 \pm 18) \times 10^3$ m^3 s^{-1} in the west out of the Weddell Sea. Combining these transports, the net mean ice export from the Weddell Sea is $(50 \pm 19) \times 10^3$ m^3 s^{-1}, corresponding to a net freshwater export due to drifting sea ice of about (0.05 ± 0.02) Sv (1 Sv = 10^6 m^3 s^{-1}). This value exceeds the freshwater export estimated for the same period by *Fahrbach et al.* [1994] and *Yaremchuk et al.* [1998] by about 20×10^3 m^3 s^{-1}. Associated

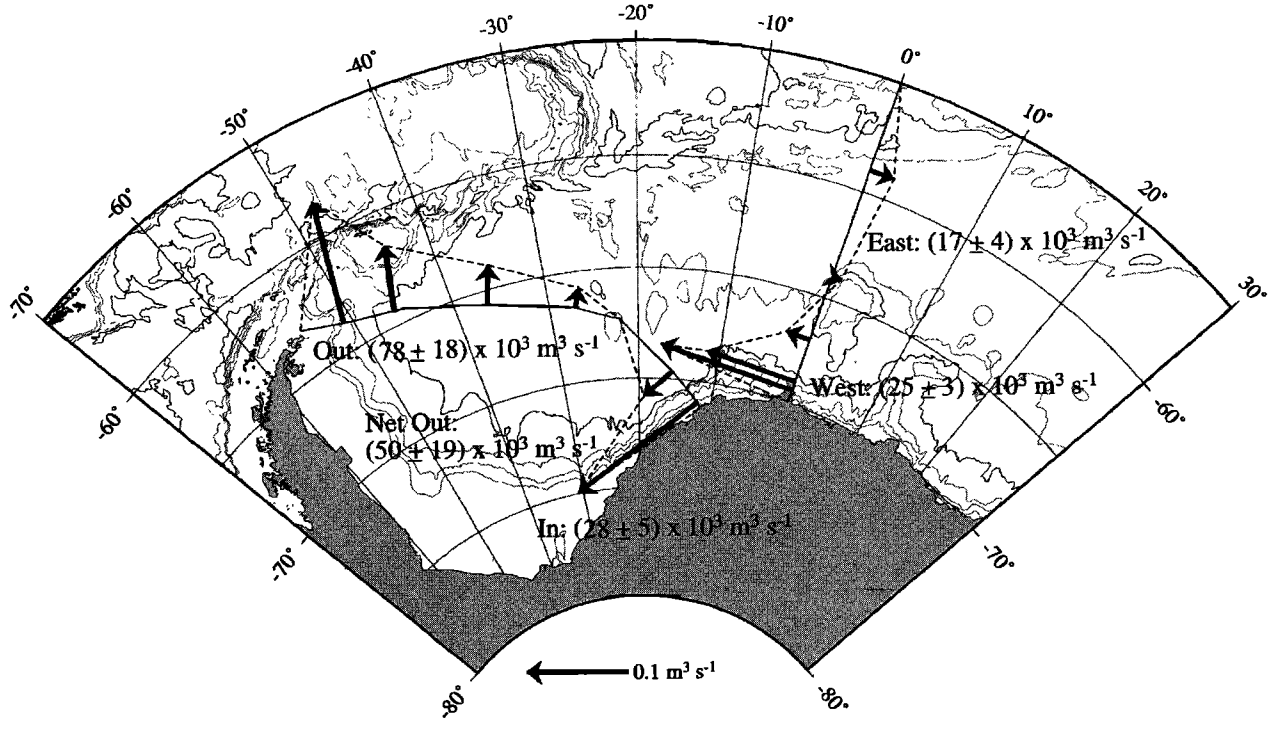

Figure 7. Integrated ice volume transport in cubic meters per second normal to the transects. The ice volume transport at each mooring location is estimated according to equation (4) and averaged over the whole deployment period.

Table 6. Integrated Ice and Salt Transports Normal to the Transects

	Ice Volume Transport, $\times 10^3$ m^3 s^{-1}		Ice Mass Transport, $\times 10^6$ kg s^{-1}		Salt Mass Transport, $\times 10^4$ kg s^{-1}		Salt$_{34.4}$ Mass Transport,[a] $\times 10^5$ kg s^{-1}	
	All Drafts	Drafts $\leq$10 m	All Drafts	Drafts $\leq$10 m	All Drafts	Drafts $\leq$10 m	All Drafts	Drafts $\leq$10 m
				Western Transect				
Southwest	28 ± 5	27 ± 5	25 ± 5	24 ± 4	12 ± 4	11 ± 3	-7 ± 2	-7 ± 2
North	78 ± 18	75 ± 17	71 ± 16	68 ± 16	32 ± 13	31 ± 12	-21 ± 5	-20 ± 5
Net	50 ± 19	48 ± 18	46 ± 17	44 ± 17	20 ± 14	20 ± 12	-14 ± 5	-13 ± 5
				Eastern Transect				
West	25 ± 3	21 ± 3	23 ± 3	19 ± 3	13 ± 2	10 ± 2	-8 ± 1	-6 ± 1
East	17 ± 4	15 ± 4	16 ± 3	14 ± 3	10 ± 2	9 ± 2	-5 ± 1	-4 ± 1

[a]The salt$_{34.4}$ mass transport is identical with $M_{S_{34.4}}$ in equation (6).

with the observed net transport of ice volume is a net northward transport of salt of $(2.0 \pm 1.4) \times 10^5$ kg s^{-1}. This transport, however, is negligible in comparison with the net amount of salt released to the ocean by sea ice formation ($(14 \pm 5) \times 10^5$ kg s^{-1}; Table 6). Taking typical summer surface salinities (33.80) as reference, the net amount of salt released to the ocean would be $(12 \pm 5) \times 10^5$ kg s^{-1}. Thus the salt needed to raise the salinity of the summer mixed layer up to that of the Winter Water amounts to about 2×10^5 kg s^{-1}, which is small in comparison with to the total amount of salt released during sea ice formation. Second, we consider the case when drafts larger than 10 m are excluded from the analysis. Except at AWI-206, the resulting transport estimates do not differ significantly from those obtained from the full-range drafts (Table 5).

Uncertainties in the transport estimates arise from statistical errors in the quantities that enter the transport calculation and from insufficient horizontal resolution of the measurements. Errors associated with the first are calculated by assuming Gaussian error propagation and are listed together with the transport estimates in Tables 5 and 6. Errors arising from insufficient data density occur in regions where changes in sea ice thickness and drift are nonlinear. These errors are hard to quantify on the basis of existing data. While we do not expect significant errors in the interior where, owing to the sea ice drift, the applied time average smoothes spatial differences, the extrapolation from the ULS nearest the coast to the coast represents a significant source of uncertainty. As a worst case estimate, we calculated transports under the assumption that, first, the ice transport remains constant between the ULS nearest the coast and the coast and, second, the ice transport vanishes inshore of the ULS closest to the coast. The resulting range in integrated ice volume transport is $\pm 2 \times 10^3$ m^3 s^{-1} at the eastern inflow and $\pm 13 \times 10^3$ m^3 s^{-1} at the western outflow.

So far we have ignored the effect of the snow cover on the sea ice transport estimates. The ULS measures the draft of an ice floe, disregarding if this ice is formed from seawater or snow. Snow on top of sea ice may affect the draft in two ways. First, the snow weights down the ice floe and increases the draft. This effect is taken into account by using the relationship presented in equation (2), assuming that snow depths are comparable between the thickness drilling and the ULS data sets. Second, if the snow/ice interface is depressed below the waterline, seawater floods the base of snow and produces slush. If the slush freezes, then layers of snow ice are added to the ice column. Flooding, controlled by the ice thickness distribution, will diminish as the ice thickness increases in relation to the snow.

The contribution of snow ice to the total ice thickness in the eastern and central Weddell Sea was first examined by *Lange et al.* [1990]. Their results show that meteoric ice amounts to about 3% of the overall mass of first-year sea ice in this region. On the basis of samples taken along the same sections covered by the ULS measurements, *Eicken et al.* [1995] find the fraction of meteoric ice to the total ice thickness to increase from 3% for first-year ice to 5% for second-year ice. Snow ice is formed from the congelation of meteoric ice and seawater and brine. Hence a meteoric ice fraction of 3% to 5% actually corresponds to a snow ice fraction of 6% to 9% for first-year ice and 10% to 15% for second-year ice. Thus the freshwater fluxes derived here may be underestimated by as much as 9% for first-year ice and 15% for second-year ice. This variation lies within the error bounds of our estimates (compare Tables 5 and 6).

6. Interannual Variations

The derived transports are based on two-year-long time series. Because multiyear (>2 years) time series of ice draft do not exist for the Weddell Sea, we are not able to estimate how representative the obtained values are with respect to other years on the basis of ice draft measurements alone. Model results suggest that interannual variations in ice export from the Weddell Sea are large. On the basis of a large-scale dynamic-thermodynamic sea ice model, *Harder and Fischer* [1999] estimated an ice export from the Weddell Sea of 1693 km^3 yr^{-1} (54×10^3 m^3 s^{-1}) in 1986 and 2339 km^3 yr^{-1} (74×10^3 m^3 s^{-1}) in 1987. *Uotila et al.* [2000] combine observations of sea ice drift

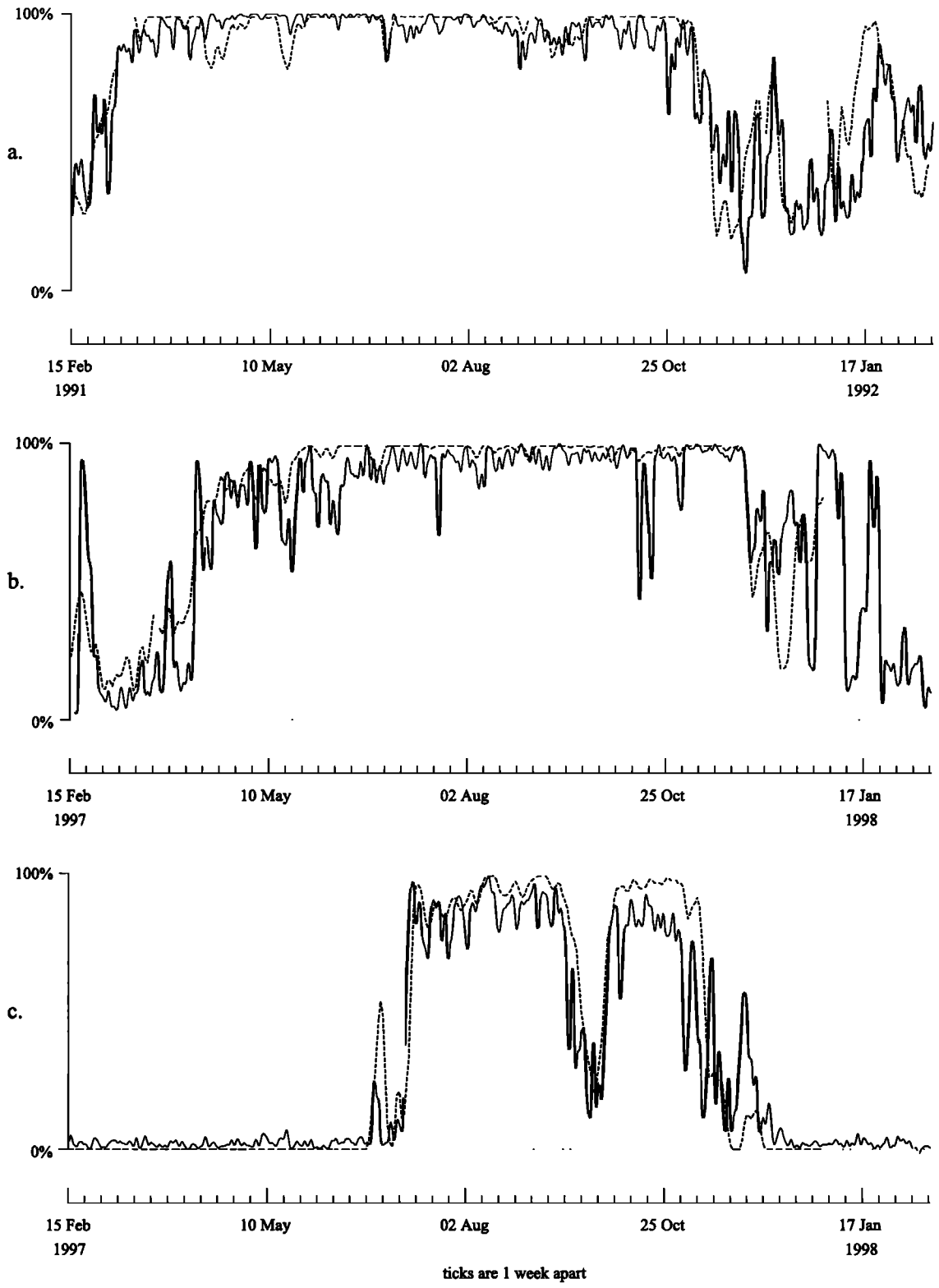

Figure 8. Year-long time series of ice coverage measured by the ULS (solid line) and by satellite (SSM/I, dashed line) at mooring locations (a) 207, (b) 233, and (c) 227.

obtained in 1996 with monthly mean ice drafts measured in 1991/1992 and report an ice export for 1996 of 1600 $km^3\ yr^{-1}$ ($51 \times 10^3\ m^3\ s^{-1}$).

Because basin-wide measurements of sea ice coverage derived from the satellite passive microwave data have been obtained since the late 1970s, we used this long-term data set to assess the interannual variability of the sea ice export. The remotely sensed sea ice concentrations, averaged over a 25 by 25 km area, agree well with the ULS point measurements. As examples, year-long time series of sea ice coverage from three selected mooring sites in different regions and during different

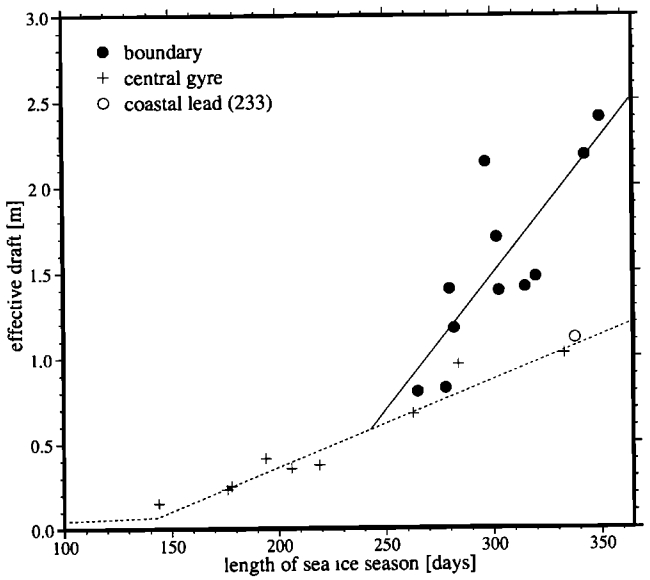

Figure 9. Empirical relationship between the length of the sea ice season, τ, measured by satellite (SSM/I) at the ULS position and annual mean effective ice draft, $\overline{d}_{\text{eff}}$, measured by the ULSs. The length of the sea ice season is defined as the number of days per year with the sea ice concentration exceeding 15%. One year spans the time period February 15 of one year to February 14 of the following year. On the basis of these observations, annual mean effective ice draft in the Weddell Sea increases approximately linearly with the length of the sea season according to equation (7).

years are displayed in Figure 8. There is generally good agreement between sea ice concentration estimates from the two sensors, suggesting that time averaging of local ULS measurements provides similar information on the sea ice fields to that obtained from spatially averaged remotely sensed data.

In order to extend the available time series of ice draft by use of the satellite passive microwave observations, we investigated if there are correlations between the annual mean effective draft and properties of the sea ice which can be derived from the SSM/I data. There is no obvious relationship between the sea ice concentration and effective draft; however, we found a clear relationship between the length of the sea ice season at a given point, defined as the number of days per year with the sea ice concentration exceeding 15%, and the annual mean effective draft. As a first estimate it results that, for a particular area in the Weddell Sea defined by our measurement sites, the length of the sea ice season, τ, and annual mean effective draft, $\overline{d}_{\text{eff}}$, are linearly related (Figure 9, Table 7). In the boundary regions of the gyre,

$$\overline{d}_{\text{eff, boundary}} = -3.286 + 0.016\,\tau \qquad (7a)$$

($r^2 = 0.66$), and for the central areas of the Weddell Sea

$$\overline{d}_{\text{eff, center}} = -0.662 + 0.005\,\tau \quad \tau \geq 143\text{days}, \qquad (7b)$$

$$\overline{d}_{\text{eff, center}} = 0.001\,\tau \quad \tau < 143\text{days} \qquad (7c)$$

($r^2 = 0.96$), where the overbar denotes annual mean quantities. From the positions of the moorings it is obvious that the mean effective ice draft is strongly affected by the presence of open water over the location. This is also evident from the time series shown in Figure 8. Hence it is not too surprising to see a strong dependence of $\overline{d}_{\text{eff}}$ on the duration of the sea ice season, τ. However, our results indicate that a similar (linear) relationship exists between τ and the annual mean ice draft $\overline{d}$ (not shown). It follows that the longer the ice formation season, the more ice can be formed and/or piled up by ridging and rafting to build up a thicker ice cover. This requires the presence of open water areas in which new ice can be continuously formed. Open water is frequently observed at our measurement sites with the ULSs, and is also confirmed by the remotely sensed sea ice concentrations which rarely reach 100%.

The above results imply that the available ice volume increases with the length of the ice-covered season. This suggests that the ice volume transport out of the area increases as well. We therefore sought an empirical relationship between the length of the sea ice season, τ, and the annual mean ice volume transport, $\overline{\Phi}$. In regions where the mean ice thickness and ice drift change proportionally to each other (compare Figures 4a and 4c), τ and $\overline{\Phi}$ are approximately related according to

Table 7. Annual Mean Quantities Used to Establish Empirical Relationships Between the Length of the Sea Ice Season (τ), Effective Ice Draft (d_{eff}), and Ice Volume Transport ($\Phi_\perp$)[a]

Mooring	Year	Coverage >15%, days	Effective Draft, m	Ice Transport, $\times 10^{-3}$ m^3 s^{-1}
207	1991	350	2.40 ± 0.04	143 ± 26
	1992	297	2.14 ± 0.03	116 ± 22
	1996	280	1.40 ± 0.03	73 ± 16
	1997	315	1.41 ± 0.03	97 ± 14
217	1991	320	1.47 ± 0.03	74 ± 15
	1992	303	1.39 ± 0.04	63 ± 16
208	1993	284	0.96 ± 0.01	43 ± 11
	1994	333	1.02 ± 0.03	45 ± 9
209	1993	263	0.67 ± 0.01	24 ± 8
210	1991	278	0.82 ± 0.02	-44 ± 9
	1992	265	0.80 ± 0.01	-34 ± 8
212	1991	343	2.18 ± 0.04	-178 ± 25
	1992	302	1.70 ± 0.04	-131 ± 19
233	1997	338	1.11 ± 0.03	-124 ± 12
232	1996	282	1.17 ± 0.03	-81 ± 11
231	1996	219	0.37 ± 0.01	-20 ± 5
	1997	206	0.35 ± 0.01	-14 ± 4
229	1996	178	0.24 ± 0.01	6 ± 2
	1997	194	0.41 ± 0.01	14 ± 4
227	1996	176	0.23 ± 0.01	32 ± 6
	1997	144	0.15 ± 0.01	20 ± 5

[a]The length of the sea ice season is defined as the number of days per year with the ice coverage exceeding 15%. Multiyear-long time series of ice coverage at the mooring sites are derived from the Special Sensor Microwave Imager (SSM/I) data.

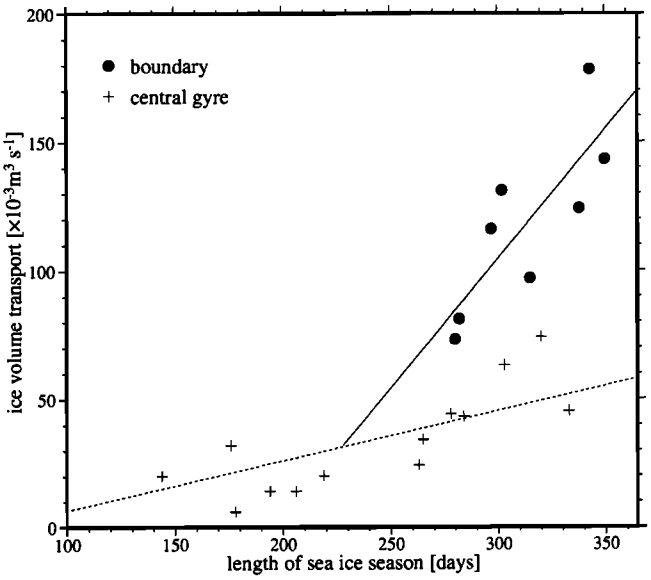

Figure 10. Empirical relationship between the length of the sea ice season, τ, measured by satellite (SSM/I) and annual mean ice volume transport, $\overline{\Phi}$, at the ULS positions. The length of the sea ice season is defined as the number of days per year with the sea ice concentration exceeding 15%. One year spans the time period February 15 of one year to February 14 of the following year. On the basis of these observations, the annual mean ice volume transport in the Weddell Sea is related to the length of the sea ice season according to equation (8).

$$\overline{\Phi}_{\text{boundary}} = -197.295 + 1.006\,\tau \qquad (8a)$$

($r^2 = 0.65$) near the boundaries and

$$\overline{\Phi}_{\text{center}} = -12.899 + 0.194\,\tau \qquad (8b)$$

($r^2 = 0.64$) in the central gyre (Figure 10, Table 7). In the northeastern Weddell Sea, ice thickness and ice drift change inversely in proportion to each other. Here, equation (8) underestimates the real transport. By using these empirical relationships, first estimates of annual mean effective drafts and ice transports can be derived basin-wide for the Weddell Sea retrospective to the advent of satellite-based microwave imagery.

Estimates of annual mean ice volume transports, integrated across the transects, are derived for the period February 1979 through February 1999. The annual mean ice transports are subject to significant interannual fluctuations. Interannual variations in ice transport in the eastern Weddell Sea amount to 11% of the average (Table 8). Integrated southwestward ice transports range from 20×10^3 m^3 s^{-1} to 30×10^3 m^3 s^{-1}. The 20-year mean southwestward ice transport is 27×10^3 m^3 s^{-1}, which agrees with the estimate presented in section 5. Integrated transport estimates off Kapp Norvegia and at the Greenwich meridian south of Maud Rise agree within the confidence limits, suggesting that the 1991/1992 and 1996/1997 results in the southeastern Weddell Sea can be combined and presented as a whole. Interannual variations in ice transport in the western Weddell Sea amount to 10% of the average. Integrated northward ice transports range from 58×10^3 m^3 s^{-1} to 85×10^3 m^3 s^{-1}, with a mean of 72×10^3 m^3 s^{-1}. The net ice export from the Weddell Sea varies by 15% during the 20-year period. Integrated ice exports range from 33×10^3 m^3 s^{-1} to 56×10^3 m^3 s^{-1} (Figure 11). The mean ice export is 46×10^3 m^3 s^{-1}, which is close to the estimate presented in section 5. Allowing for a ±10% variation in satellite-derived sea ice concentration, prescribed by the accuracy of the satellite sensors, the integrated ice volume transports deduced from the empirical relationships may vary by as much as $\pm 4 \times 10^3$ m^3 s^{-1} in the eastern inflow, $\pm 5 \times 10^3$ m^3 s^{-1} in the western outflow, and $\pm 6 \times 10^3$ m^3 s^{-1} in the net outflow. We conclude that in spite of a significant interannual variability of the ice transport, the temporal and spatial distributions of the ULS measurements do not significantly affect our results, but that the observations are representative for a longer term (20 years) mean.

7. Discussion

The export of sea ice and the associated brine release during freezing, the freshwater input through the melting of sea ice and continental ice, the combined effects of precipitation and evaporation, the export of dense

Table 8. Interannual Variations of the Integrated Ice Volume Transport From 1979 to 1998[a]

	1979	1980	1981	1982	1983	1984	1985	1986	1987	1988	1989	1990	1991	1992	1993	1994	1995	1996	1997	1998	Mean	σ
Western Transect																						
Southwest	30	27	24	30	27	27	28	28	23	23	20	29	29	23	23	27	25	30	30	26	27	3
North	80	79	65	69	73	69	58	76	69	75	72	75	85	69	64	81	74	63	73	70	72	7
Net	50	52	41	39	46	42	30	48	46	52	52	46	56	46	41	54	49	33	43	44	46	7
Eastern Transect																						
West	29	23	20	23	22	29	23	28	22	18	24	27	27	23	30	26	28	27	23	18	25	4
East[b]	(21)	(18)	(20)	(14)	(15)	(18)	(20)	(14)	(20)	(19)	(15)	(8)	(15)	(18)	(15)	(18)	(19)	(19)	(17)	(17)	(17)	(3)

[a]Standard deviation, σ. The numbers $\times 10^3$ yield the integrated volume transports in m^3 s^{-1}.
[b]The empirical relationship, presented in equation (8), does not yield accurate transport estimates for stations along the Greenwich meridian north of Maud Rise, since here the effective ice draft and the ice drift are inversely proportional to each other.

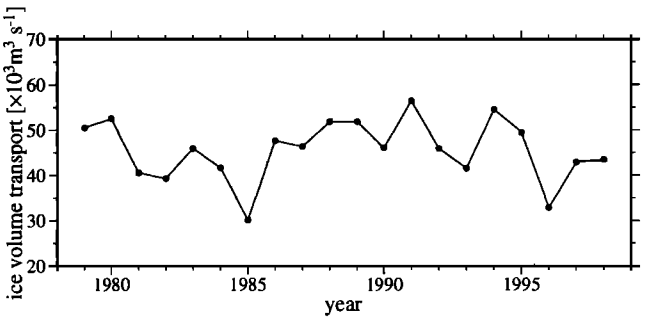

Figure 11. Annual mean ice export from the Weddell Sea from 1979 to 1998 derived from the empirical relationships presented in equation (8). The means were calculated over the period February 15 of one year to February 14 of the following year.

Weddell Sea Bottom Water out of the region, and the advection of fresher water from the east with the cyclonic gyre circulation all contribute to the freshwater budget of the Weddell Sea. In this section we try to assess the relative importance of each of these components to the total freshwater budget.

In this study the net mean freshwater export from the Weddell Sea due to drifting sea ice is estimated to $(50 \pm 19) \times 10^3$ m^3 s^{-1}. Since there is no essential loss or gain of salt south of the western transect, this freshwater export leads to a salinity increase of the outflowing water, or it must be balanced by the other components of the freshwater budget. *Jacobs et al.* [1992] estimate that more than 200 km^3 yr^{-1}, corresponding to about 6.3×10^3 m^3 s^{-1}, melt from the Filchner-Ronne Ice Shelf base alone. *Lange* [1987] estimates a discharge rate of 150 km^3 yr^{-1} (4.5×10^3 m^3 s^{-1}) across the Filchner-Ronne Ice Shelf Front. Taking into account refreezing at the bottom of the ice shelf, *Grosfeld and Gerdes* [1998] show that the net freshwater input from the Filchner-Ronne Ice Shelf is only about 90 km^3 yr^{-1} (2.9×10^3 m^3 s^{-1}). Freshwater inputs from the other ice shelves, i.e., the eastern Weddell ice shelves and the Larsen Ice Shelf, are estimated to be 4.4×10^3 m^3 s^{-1} and 2.4×10^3 m^3 s^{-1}, respectively (H. H. Hellmer, personal communication, 1999). Combining the freshwater input from all ice shelves, the total amount of ice shelf meltwater put into the Weddell Sea south of the transect is 11×10^3 m^3 s^{-1}. In addition to the freshwater input through ice shelf melting, freshwater is put into the Weddell Sea through the melting of calved icebergs. However, some of this ice may leave the Weddell Sea and melt further north. To date, no reliable estimate on the amount of iceberg melt put into the Weddell Sea exists. The area of the Weddell Sea south of the western transect is approximately 1.8×10^{12} m^2. Based on an average precipitation-evaporation rate of 0.35 m per year [*Jaeger*, 1976; D. H. Bromwich et al., unpublished manuscript, 1997], the surplus of precipitation over evaporation in the Weddell Sea is 20×10^3 m^3 s^{-1}. As a result, the freshwater input by melting and precipitation combine to 31×10^3 m^3 s^{-1}. The remaining 19×10^3 m^3 s^{-1} can be accounted for by the formation and export of dense, newly ventilated bottom water from the Weddell Sea and by the flow of fresher water from the east.

The export of newly ventilated Weddell Sea Bottom Water (WSBW) is estimated assuming that WSBW with salinities greater than 34.64 is formed from pure Winter Water (WW) with salinities around 34.40. If no freshwater is advected into the Weddell Sea, 2.6 Sv of bottom water can be formed. Since 34.40 is certainly an upper bound for the salinity of WW, observed only at the end of the winter when most of the sea ice has already been formed, and since it is also likely that some freshwater is advected into the region, the 2.6 Sv give an upper bound for the bottom water formation rate in the Weddell Sea. While this is significantly less than the widely accepted ventilation rates of the deep sea, it agrees with previously derived estimates [*Fahrbach et al.*, 1995, 2000].

We have derived long-term time series of annual mean sea ice transports in the Weddell Sea on the basis of the empirical relationship established between the ULS-derived sea ice transports and the sea ice season lengths obtained from satellite passive microwave data. One has to realize that the quantification of the sea ice transports by the duration of the length of the sea ice season is physically a simplified approach because the demonstrated relationships between ULS-derived ice thicknesses and transports and satellite data are limited by the highly variable regional and seasonal characteristics of Weddell Sea ice. This variability is in part responsible for the fact that the derived sea ice export and related freshwater fluxes depend very much on the definition of the study region, dictated by the locations of the moorings. During years in which the ice edge is located south of the western line of moorings most of the time, the freshwater export from the Weddell Sea would be underestimated because variations in the mixed layer freshwater budget controlled by ice melt just south of the line of moorings are not taken into account. Conversely, a heavy ice year with the ice edge located north of the mooring line most of the time would result in a highly unbalanced estimate of the freshwater budget. Thus future calculations of net ice volume transports and related freshwater fluxes will require continued seasonal to interannual measurements of sea ice draft and drift from moored sensors such that a more detailed assessment of the import and export of freshwater derived from ice melt and growth may be derived and accurate satellite- and model-derived proxy records for ice drift and ice thickness can be developed.

Acknowledgments. The successful acquisition of the large variety of data utilized in this study was made possible only through the efforts of a great many people. Special thanks are due Gerd Rohardt and Ekkehard Schütt and the officers and crew of the R/V *Polarstern*. We are grateful to Ralph Timmermann, who provided the mixed layer pa-

rameters used to compute the vertical sound velocity profiles above the ULSs. The ice core and thickness drilling data used to convert ice draft to ice thickness and to estimate the mean salinity of ice floes were kindly provided by Hajo Eicken. Christoph Kottmeier supplied the parameters used in the calculation of sea ice drift. The satellite passive microwave data were kindly provided by Stefan Kern and Christian Thomas of the Institute of Environmental Physics, University of Bremen, Bremen, Germany. The ECMWF data have been received by the German Weather Service, Offenbach. The paper benefited from discussions with Hartmut Hellmer and Mike Schröder. Stan Jacobs and four anonymous reviewers read the manuscript carefully and suggested numerous improvements. The paper is AWI contribution 1774.

References

Augstein, E., N. Bagriantsev, and H. W. Schenke (Eds.), The expeditions ANTARKTIS VIII/1-2 in 1989 with the Winter Weddell Gyre Study of the Research Vessels "Polarstern" and "Akademik Fedorov", *Ber. Polarforsch., 84*, 129 pp., 1991.

Bathmann, U., M. Schulz-Baldes, E. Fahrbach, V. Smetacek, and H.-W. Hubberten (Eds.), The expeditions ANTARKTIS IX/1-4 of the Research Vessel "Polarstern" in 1990/91, *Ber. Polarforsch., 100*, 403 pp., 1992.

Bathmann, U., V. Smetacek, H. de Baar, E. Fahrbach, and G. Krause (Eds.), The expeditions ANTARKTIS X/6-8 of the Research Vessel "Polarstern" in 1992/93, *Ber. Polarforsch., 135*, 236 pp., 1994.

Brennecke, W., Die ozeanographischen Arbeiten der Deutschen Antarktischen Expedition 1911-1912, in *Arch. Dtsch. Seewarte, 39*, 216 pp., 1921.

Cavalieri, D. J., The validation of geophysical products using multisensor data, in *Microwave Remote Sensing of Sea Ice, Geophys. Monogr. Ser.*, vol. 68, edited by F. Carsey, pp. 233-242, AGU, Washington, D. C., 1992.

Comiso, J. C., T. C. Grenfell, M. Lange, A. W. Lohanick, R. K. Moore, and P. Wadhams, Microwave remote sensing of the Southern Ocean ice cover, in *Microwave Remote Sensing of Sea Ice, Geophys. Monogr. Ser.*, vol. 68, edited by F. Carsey, pp. 243-259, AGU, Washington, D. C., 1992.

Deacon, G. E. R., A general account of the hydrology of the South Atlantic Ocean, in *Discovery Rep., 7*, 171-238, 1933.

Eicken, H., Salinity profiles of Antarctic sea ice: Field data and model results, *J. Geophys. Res., 97*, 15,545-15,557, 1992.

Eicken, H., Deriving modes and rates of ice growth in the Weddell Sea from microstructural, salinity and stable-isotope data, in *Antarctic Sea Ice: Physical Processes, Interactions and Variability, Antarct. Res. Ser.*, vol. 74, edited by M. O. Jeffries, pp. 89-122, AGU, Washington, D. C., 1998.

Eicken, H., M. A. Lange, and G. S. Dieckmann, Spatial variability of sea-ice properties in the northwestern Weddell Sea, *J. Geophys. Res., 96*, 10,603-10,615, 1991.

Eicken, H., M. A. Lange, H.-W. Hubberten, and P. Wadhams, Characteristics and distribution patterns of snow and meteoric ice in the Weddell Sea and their contribution to the mass balance of sea ice, *Ann. Geophys., 12*, 80-93, 1994.

Eicken, H., H. Fischer, and P. Lemke, Effects of the snow cover on Antarctic sea ice and potential modulation of its response to climate change, *Ann. Glaciol., 21*, 369-376, 1995.

European Centre for Medium-Range Weather Forcasts, The description of the ECMWF/WCRP level III-A Global Atmospheric Data Archive, Reading, England, UK, 1992.

Fahrbach, E. (Ed.), The expedition ANTARKTIS XV/4 of the research vessel "*Polarstern*" in 1998, *Ber. Polarforsch., 314*, 109 pp., 1999.

Fahrbach, E., and D. Gerdes (Eds.), The expeditions ANTARKTIS XIII/4-5 of the research vessel "*Polarstern*" in 1996, *Ber. Polarforsch., 239*, 126 pp., 1997.

Fahrbach, E., G. Rohardt, M. Schröder, and V. H. Strass, Transport and structure of the Weddell Gyre, *Ann. Geophys., 12*, 840-855, 1994.

Fahrbach, E., G. Rohardt, N. Scheele, M. Schröder, V. H. Strass, and A. Wisotzki, Formation and discharge of deep and bottom water in the northwestern Weddell Sea, *J. Mar. Res., 53*(4), 515-539, 1995.

Fahrbach, E., S. Harms, G. Rohardt, M. Schröder, and R. Woodgate, The flow of bottom water in the northwestern Weddell Sea, *J. Geophys. Res.*, in press, 2001.

Gloersen, P., W. J. Campbell, D. J. Cavalieri, J. C. Comiso, C. L. Parkinson, and H. J. Zwally, *Arctic and Antarctic Sea Ice, 1978-1987: Satellite Passive Microwave Observations and Analysis, Spec. Publ. 511*, 290 pp., NASA, Washington, D. C., 1992.

Gordon, A. L., Oceanography of Antarctic waters, in *Antarct. Oceanology I, Antarctic Res. Ser.*, vol. 15, edited by J. L. Reid, pp. 169-203, AGU, Washington, D. C., 1971.

Grosfeld, K., and R. Gerdes, Circulation in the Filchner-Ronne ice shelf domain: First results from a 3D-ocean model, in *Filchner-Ronne Ice Shelf Programme (FRISP), Rep. 12*, edited by H. Oerter, pp. 35-39, Alfred-Wegener-Inst. for Polar and Mar. Res., Bremerhaven, Germany, 1998.

Harder, M., and H. Fischer, Sea ice dynamics in the Weddell Sea simulated with an optimized model, *J. Geophys. Res., 104*, 11,151-11,162, 1999.

Heygster, G., L. T. Pedersen, J. Turner, C. Thomas, T. Hunewinkel, H. Schottmüller, and T. Viehoff, PELICON: Project for Estimation of Long-Term Variability of Ice Concentration, final report, *EC Contract Rep. EV5V-CT93-0268 (DG 12)*, 188 pp., Bremen, Germany, 1996.

Hoeber, H., Sea ice dynamics in the Weddell Sea in winter, *Ann. Geophys., 15*, 9-16, 1991.

Jacobs, S. S., H. H. Hellmer, C. S. M. Doake, A. Jenkins, and R. M. Frolich, Melting of ice shelves and the mass balance of Antarctica, *J. Glaciol., 38*(130), 375-387, 1992.

Jaeger, L., Monatskarten des Niederschlags für die ganze Erde, *Ber. Dtsch. Wetterdienstes, 139*, 1-38, 1976.

Johannessen, A. A., CMI ES-300 user's guide, 10 pp., Christian-Michelsen Res. Inst., Bergen, Norway, 1995.

Kottmeier, C., and L. Sellmann, Atmospheric and oceanic forcing of Weddell Sea ice motion, *J. Geophys. Res., 101*, 20,809-20,824, 1996.

Kottmeier, C., J. Olf, W. Frieden, and R. Roth, Wind forcing and ice motion in the Weddell Sea region, *J. Geophys. Res., 97*, 20,373-20,383, 1992.

Lange, M. A., Quantitative estimates of the mass flux and the ice movement along the ice edges in the eastern and southern Weddell Sea, in *Dynamics of the West Antarctic Ice Sheet*, edited by C. J. van der Veen and J. Oerlemans, pp. 57-74, D. Reidel, Norwell, Mass., 1987.

Lange, M. A., and H. Eicken, The sea ice thickness distribution in the northwestern Weddell Sea, *J. Geophys. Res., 96*, 4821-4837, 1991.

Lange, M. A., P. Schlosser, S. F. Ackley, P. Wadhams, and G. S. Dieckmann, ^{18}O concentrations in sea ice of the Weddell Sea, Antarctica, *J. Glaciol., 36*, 315-323, 1990.

Lemke, P. (Ed.), The expedition ANTARKTIS X/4 of the research vessel "*Polarstern*" in 1992, *Ber. Polarforsch., 140*, 90 pp., 1994.

Lothe, T., CMI ES-300 model VIII operating manual, 24 pp., Christian-Michelsen Res. Inst., Bergen, Norway, 1997.

Mantyla, A. W., and J. L. Reid, Abyssal characteristics of the world ocean waters, *Deep Sea Res., Part I, 30*, 805-833, 1983.

Martinson, D. G., and C. Wamser, Ice drift and momentum exchange in winter Antarctic pack ice, *J. Geophys. Res., 95*, 1741-1755, 1990.

Mosby, H., The water of the Atlantic Ocean, in *Scientific Results of the Norwegian Antarctic Expedition*, vol. 1, pp. 1-131, 1934.

Parkinson, C. L., Length of the sea ice season in the Southern Ocean, 1988-1994, in *Antarctic Sea Ice: Physical Processes, Interactions and Variability, Antarct. Res. Ser.*, vol. 74, edited by M. O. Jeffries, pp. 173-186, AGU, Washington, D. C., 1998.

Reid, J. L., and R. J. Lynn, On the influence of the Norwegian-Greenland and Weddell Seas upon the bottom waters of the Indian and Pacific Oceans, *Deep Sea Res., Part I, 18*, 1063-1088, 1971.

Schröder, M., and E. Fahrbach, On the structure and the transport of the eastern Weddell Gyre, *Deep Sea Res., Part I, 46*, 501-527, 1999.

Strass, V. H., Measuring ice draft and coverage with moored upward looking sonars, *Deep Sea Res., Part I, 45*, 785-818, 1998.

Strass, V. H., and E. Fahrbach, Temporal and regional variation of sea ice draft and coverage in the Weddell Sea obtained from upward looking sonars, in *Antarctic Sea Ice: Physical Processes, Interactions and Variability, Antarct. Res. Ser.*, vol. 74, edited by M. O. Jeffries, pp. 123-139, AGU, Washington, D. C., 1998.

Thorndike, A. S., and R. Colony, Sea ice motion in response to geostrophic winds, *J. Geophys. Res., 87*, 5845-5852, 1982.

Timmermann, R., P. Lemke, and C. Kottmeier, Formation and maintenance of a polynya in the Weddell Sea, *J. Phys. Oceanogr., 29*(6), 1251-1264, 1999.

Uotila, J., T. Vihma, and J. Launiainen, Response of the Weddell Sea pack ice to wind forcing, *J. Geophys. Res., 105*, 1135-1151, 2000.

Vihma, T., and J. Launiainen, Ice drift in the Weddell Sea in 1990-1991 as tracked by a satellite buoy, *J. Geophys. Res., 98*, 14,471-14,485, 1993.

Vihma, T., J. Launiainen, and J. Uotila, Weddell Sea ice drift: kinematics and wind forcing, *J. Geophys. Res., 100*, 18,503-18,515, 1995.

Wadhams, P., Sea ice thickness changes and their relation to climate, in *The Polar Oceans and Their Role in Shaping the Global Environment, Geophys. Monogr. Ser.*, vol. 85, edited by O. M. Johannessen, R. D. Muench, and J. E. Overland, pp. 337-361, AGU Washington, D. C., 1994.

Wadhams, P., M. A. Lange, and S. F. Ackley, The ice thickness distribution across the Atlantic sector of the Antarctic Ocean in midwinter, *J. Geophys. Res., 92*, 14,535-14,552, 1987.

Wadhams, P., C. B. Sear, D. R. Crane, M. A. Rowe, S. J. Morrison, and D. W. S. Limbert, Basin-scale ice motion and deformation in the Weddell Sea during winter, *Ann. Geophys., 12*, 178-186, 1989.

Wüst, G., Das Bodenwasser und die Gliederung der Atlantischen Tiefsee, *Wiss. Ergebn. Dtsch. Atlant. Exped. Meteor 1925-1927, 6*(1), 1-106, 1933.

Yaremchuk, M., D. Nechaev, J. Schröter, and E. Fahrbach, A dynamically consistent analysis of circulation and transports in the southwestern Weddell Sea, *Ann. Geophys., 16*, 1024-1038, 1998.

Zwally, H. J., J. C. Comiso, C. L. Parkinson, W. J. Campbell, F. D. Carsey, and P. Gloersen, Antarctic sea ice 1973-1976: Satellite passive microwave observations, NASA Spec. Publ., *SP-459*, 1983.

S. Harms, Institut für Meereskunde an der Universität Kiel, Düsternbrooker Weg 20, 24105 Kiel, Germany. (sharms@ifm.uni-kiel.de)

E. Fahrbach and V. H. Strass, Alfred-Wegener-Institut für Polar- und Meeresforschung, Postfach 12 01 61, 27515 Bremerhaven, Germany. (efahrbach@awi-bremerhaven.de; vhstrass@awi-bremerhaven.de)

(Received July 20, 1999; revised March 27, 2000;
accepted July 5, 2000.)